

J. ADAMIEC\* , S. MUCHA\*

## DETERMINATION BRITTLE TEMPERATURE RANGE OF MSR-B MAGNESIUM ALLOY

### OKREŚLENIE ZAKRESU KRUCHOŚCI WYSOKOTEMPERATUROWEJ STOPU MAGNEZU MSR-B

Magnesium alloys are a part of a group of lightweight and ultra-lightweight alloys, which are important in practical use in constructions. Due to the development of these alloys, they are currently used in many fields of science and their maximum working temperature is about 250°C. Nowadays, magnesium alloys are used for casting into sand moulds of huge dimensional castings, high-pressure castings and precise casings. In castings of magnesium alloys defects or inconsistencies (such as casting misruns, porosities and cracks) often appear, particularly in huge dimensional castings. Such defects are repaired with the use of padding and welding. The welding techniques can be applied by using weld material consisting of magnesium alloy, as well as for regeneration of alloys after excessive wear. Nevertheless, the number of the repaired castings, which were permitted for use, is not satisfactory to obtain a profitable production. The main reasons for wear are the cracks appearing during welding in brittleness high-temperature range.

This work in combination with industrial tests of casting and welding shows that the causes of high-temperature brittleness are partial tears of the structure and solidification cracks of both castings and welded and padded joints. Such phenomena should be treated as irreversible failures caused by the process of crystallisation that occurs in the area of co-existence of the solid and liquid structural constituent.

This paper contains research covering: determining liquidus and solidus temperatures, determining nil-strength temperature (NST), nil-ductility temperature (NDT) and ductility recovery temperature (DRT). The obtained results enabled to define brittle temperature range of the MSR-B magnesium alloy. The brittleness is caused mainly by metallurgical factors, i.e., precipitation of inter-metal phases from the solid solution.

Microstructure of fractures was observed using a Hitachi S-3400N scanning electron microscopy (SEM). Analyses of chemical composition were performed using an energy-dispersive X-ray spectrometer (EDS), Noran System Six of Thermo Fisher Scientific and phase analysis was performed by X-ray diffraction (XRD). Essential differences of fracture morphology type in brittle temperature range were observed and described.

Stopy magnezu obok stopów aluminium i stopów tytanu wchodzą w skład grupy stopów lekkich i ultralekkich, które mają największe znaczenie praktyczne w zastosowaniach konstrukcyjnych. Ciągły rozwój stopów magnezu spowodował, że obecnie stopy te są wykorzystywane w wielu dziedzinach techniki, a ich maksymalna temperatura pracy wynosi około 250°C. Stopy magnezu stosowane są obecnie na odlewane do form piaskowych odlewy wielkogabarytowe, odlewy wysokociśnieniowe oraz odlewy precyzyjne. W odlewach ze stopów magnezu często występują wady i niezgodności odlewnicze (niedolania, rzadziny oraz pęknięcia), szczególnie w odlewach wielkogabarytowych. Wady te naprawiane są z zastosowaniem technik napawania i spawania. Techniki spawalnicze mogą być stosowane również w przypadku łączenia elementów ze stopów Mg, jak również do regeneracji odlewów po ich zużyciu eksploatacyjnym. Liczba odlewów naprawianych, dopuszczanych do eksploatacji jest niezadowalająca, co często czyni produkcję nieopłacalną. Główną tego przyczyną są pęknięcia odlewów powstające w procesie spawania w wysokotemperaturowym zakresie kruchości.

Na podstawie wyników badań wykazano, że efektem końcowym zjawiska kruchości wysokotemperaturowej są naderwania struktury i pęknięcia gorące odlewów oraz złączy spawanych i napawanych. Zjawiska te należy traktować jako nieodwracalne awarie powstałe w procesie krystalizacji tj. w obszarze współistnienia fazy stałej i ciekłej.

W pracy określono temperaturę likwidus, temperaturę solidus, temperaturę utraty wytrzymałości (NST), temperaturę utraty plastyczności (NDT) oraz temperaturę odzyskania plastyczności (DRT). Określone temperatury pozwoliły na wyznaczenie zakresu kruchości wysokotemperaturowej stopu MSR-B. O tym zakresie kruchości decydują przede wszystkim czynniki metalurgiczne tj. obecność faz międzymetalicznych na granicach roztworu stałego.

Struktury przełomów obserwowano na skaningowym mikroskopie elektronowym Hitachi S-3400N. Mikroanalizę składu chemicznego była wykonana metodą EDS w systemie Noran System SIX firmy Thermo Fisher Scientific, a analizę fazową wykonano metodą dyfrakcji promieniowania RTG (XRD).

\* SILESIA UNIVERSITY OF TECHNOLOGY, FACULTY OF MATERIALS SCIENCE AND METALLURGY, 40-019 KATOWICE, 8 KRASIŃSKIEGO STR., POLAND

## 1. Introduction

Crystallisation of alloys, both during casting or welding occurs always in some temperature range, called crystallisation range. The nuclei of crystallisation appear during lowering temperature below the liquidus one. In a pool of liquid metal the nuclei are formed in partially melted crystallites and grow usually to the form of column crystals or dendritic crystals. In a certain moment of crystallisation the crystals begin to interact between each other as long as they form a skeleton of the continuous solid phase. The temperature in which the crystals begin to interact between each other is called the coherence temperature and the temperature when the lattice of solid body starts to form - rigidity temperature. Below this temperature the semi-solid body starts to possess characteristics of the solid phase, which means that it preserves the shape and exhibits the mechanical properties – the resistance and ductility [1, 2].

Partial tears of the structure and solidification cracks of the casts and welded and padded joints are the final effect of the high-temperature brittleness phenomenon. They should be treated as irreversible failures formed during the crystallisation process, which is in the range of liquid and solid phase co-existence [1].

Solidification cracks are of inter-crystalline character and the main reason of their formation is the decrease in metal plasticity in a certain temperature range, called the brittle temperature range (BTR) and the strain, under the impact of which it will be during this particular time range. The decrease in metal ductility may be caused by the decrease in resistance of the crystallite boundaries areas, as a result of the presence of liquid film or accumulation of a big amount of defects of crystal lattice in those areas. Liquid may appear in the last phase of solidification or as a result of partial melting of the areas of crystallite boundaries during metal heating in solid stage [3].

There are three different types of solidification cracks [3]:

- solidification cracking – forming in the process of material solidification as the effect of the residual liquid film separation in the area of crystallite boundaries,
- liquation cracking – forming as a result of partial melting of the crystallite boundaries in the solid stage.
- of polygonisation type – forming as a result of micro-pores presence in the solid phase, which with the presence of static stresses and slide on the crystallite boundaries become the nuclei of solidification cracks.

Views [1,3-4] concerning designating of the upper and lower limit of the brittle temperature range vary a lot. One of the theories says that the upper limit of the BTR may correspond to the liquidus temperature ( $T_L$ ), and the lower one may be around the solidus temperature ( $T_S$ ) or, for some alloys, near the re-crystallisation temperature [3]. According to the second theory, the upper limit of the BTR is the temperature of the resistance loss – nil-strength temperature (NST), which is a temperature when the material strength goes to zero and after its exceeding the material is no longer able to transfer load. The lower limit of the BTR here is the ductility recovery temperature (DRT), defined as such a temperature during cooling in which the material ability to plastic deformation appears [4]. The aim of this study was to determine brittle temperature range and understanding of crystallization phenomena during welding of magnesium alloy MSR-B.

## 2. Research material and methodology

### 2.1. Research material

In the research a new magnesium alloy, MSR-B, was used, which includes silver and rare earth metals (RE) and zirconium. Table 1 presents the chemical composition and mechanical properties of the delivered pig sows of the MSR-B alloy. Tests were conducted for alloy in as-received condition, after ageing and after precipitation hardening. The parameters of the heat treatment are presented in Table 1.

TABLE 1  
Chemical composition, mechanical properties and heat treatment parameters of MSR-B alloy

Chemical composition, %				
Mg	Ag	Zr	RE	Inne
Reszta	2.40	0.46	2.52	< 0.05
Mechanical properties				
$R_e$ , MPa	$R_m$ , MPa	$A_5$ , %	Z, %	HV3
185	240	2	–	80 – 105
MSR-B Alternative heat treatment		HT I	Solution I: 8 h/525°C/water 60°C	
		HT II	Solution II: 8 h/525°C/water 60°C Ageing: 16 h/250°C/air	

### 2.2. Determination of the liquidus and solidus temperatures

The liquidus and solidus temperatures were determined with the use of differential thermal analysis DTA.

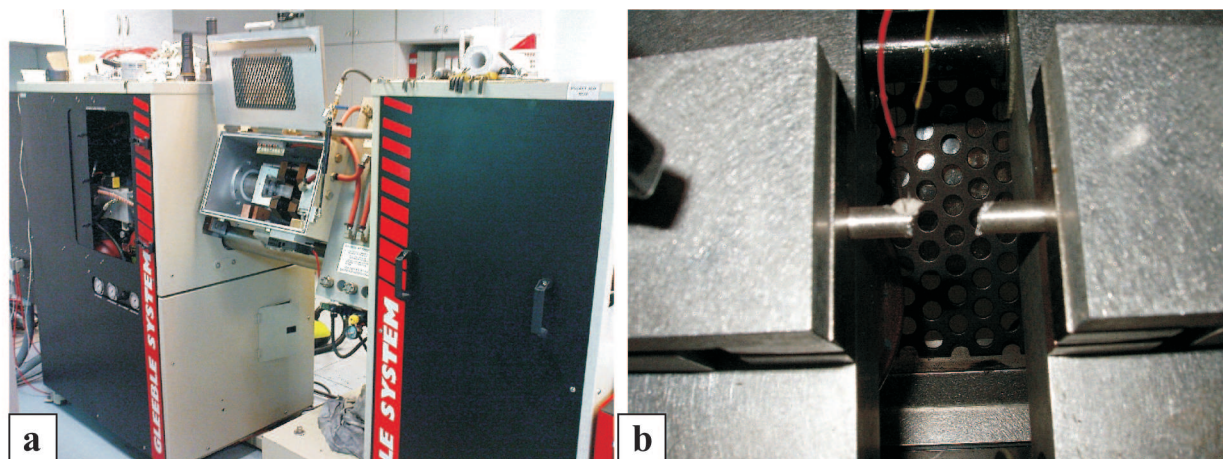


Fig. 1. a) Gleeble 3800 simulator, b) sample view after the NST test

The test was conducted on SETSYS device by SE-TARAM company. During the test, when measuring the enthalpy of the phase transition, related to melting and solidification of the tested alloy, a TG – DTA head was used.

Differential thermal analysis was conducted with the use of thermoelement type “S” Pt-Rh /Pt-Rh 10%. The tested material was placed in an argon neutral atmosphere (Ar 99,999%). The temperature of 750°C was set as the maximum heating temperature, with heating speed of 10°C/min. The speed of gas flow was 1.45 l/h. The measurement of the beginning and end of the transformation was conducted with the use of intersection of two tangents method – “one set point” method.

### 2.3. Determination of the Nil-strength temperature

NST test was conducted on cylindrical samples within the size  $\varnothing 6 \times 90$  mm, on a Gleeble 3800 simulator (Fig. 1a). Type S thermoelements were bonded to the samples and then rollers were fixed, with the use of copper grips, in the chamber of the device (Fig. 1b). The constant distance of the grips – 52.4 mm was maintained. The test consisted of application of the minimum preload of 0.6-0.7 kN, which was then maintained until the end of the experiment. Next, samples were heated with the speed of 20°C/s to the temperature of 400°C. After reaching that temperature the samples were further heated but with the speed of 1°C/s until the point when resistance loss was received. The results are presented in Table 2.

### 2.4. Determination of the nil-ductility temperature (NDT) and the ductility recovery temperature (DRT)

The NDT and DRT tests were conducted on a Gleeble 3800 simulator. The nil-ductility temperature NDT

was determined during heating of a cylindrical sample size  $\varnothing 10 \times 120$  mm in an argon atmosphere to a set temperature and next during stretching of the sample with a stated constant strain rate of (0,008 1/s and 0,16 1/s) (Fig. 2). Figure 3 presents samples after a NDT test with strain rate 0,16 1/s.

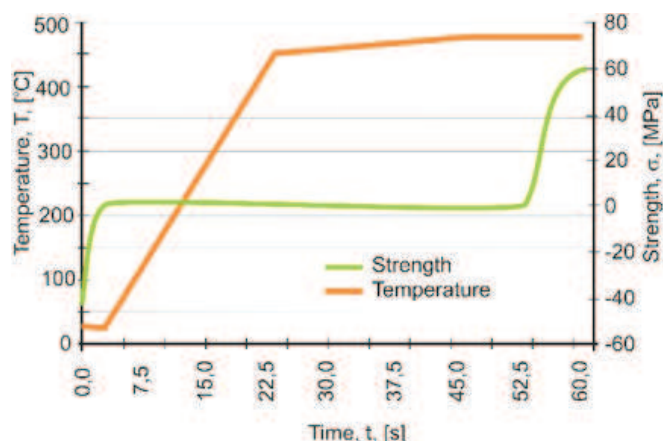


Fig. 2. Change in stress and temperature within time during NDT test, strain rate of 0,16 mm/s, temperature of 475°C

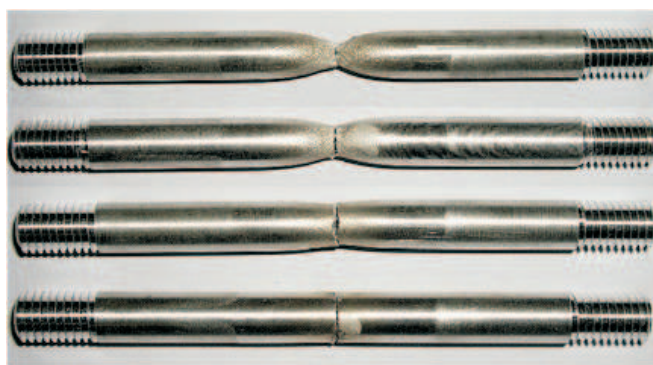


Fig. 3. Exemplary samples after NDT test, strain rate of 0,16 mm/s: a) sample deformed at 475°C, b) sample deformed at 485°C, c) sample deformed at 500°C, d) sample deformed at 520°C

The ductility recovery temperature – DRT was determined during cooling of samples from the NST range to a set value and next by applying a strain with constant strain rate of (0.008 1/s and 0.16 mm/s). Figure 4 shows the stress change and temperature change during the DRT test.

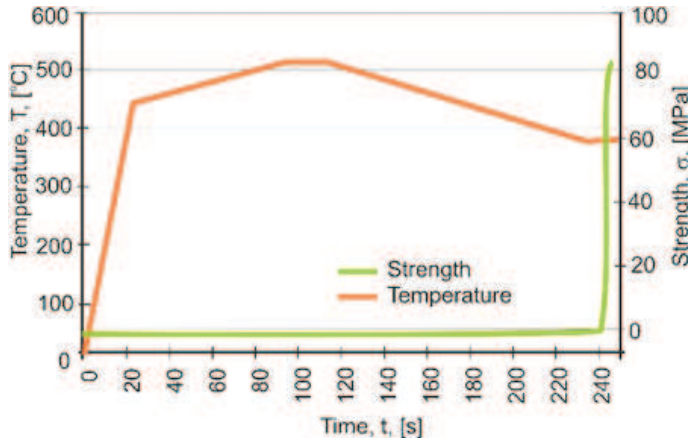


Fig. 4. Change in stress and temperature within time during DRT test, strain rate of 0.16/s, temperature of 475°C

Having conducted the tests, for each sample the diameter of contraction  $d_r$  and length increment  $\Delta l$  were measured. The Z contraction was also calculated and the stress value at rupture of sample was noted down. The measurements error did not exceed 5%. The results are presented in Tables 3 and 4.

**2.5. Metallographic and fractographic examination**

Metallographic and fractographic examination were conducted in order to determine the mechanism of solidification cracks formation. Macrostructure observations were conducted on Olympus SZX-9 stethoscope mi-

croscope, in dark field technique, with magnifications of 3-10x, whereas the microstructure observations were conducted by means of a light microscope (LM) Olympus GX71, in bright field technique, with magnifications from 50 to 500x (Fig. 8-10). Metallographic examination on light microscope were complemented with observations of micro-sections and the crack surface on a scanning electron microscope (SEM) HITACHI S-3400N, with the use of observation techniques of secondary electrons (SE) and observation technique of back-scattered electrons (BSE) (Figs. 8-10). The SE technique allowed topography analysis of the crack surface, whereas the BSE observation technique allowed determination of differences in the average chemical composition of the tested areas. Identification of intermetallic phase was basing on results of chemical composition of MSR-B welded joint, which was performed with the help of scanning microscope HITACHI S-4200 equipped with the system of X-ray microanalysis VOYAGER together with EDS spectrometer. As the test supplementation, the phase analysis was performed by the method of X-ray diffraction on polycrystals. Examinations were made with use of diffractometer JDX-7S of Japanese JEOL Co., having vertical focusing system. The source of radiation was a lamp with copper anode, supplied with direct tension 40 kV at 20 mA current. Monochromatization of beam was performed at graphite monochromator. The range and time constant of integrator was chosen in such a way that a maximum isolation of diffraction lines out of background has been achieved. The phase identification was accomplished with the help of PCSIWIN software, utilizing a database in form of master file JCPDS – International Centre for Diffraction Data 2000. The results of EDS and XRD analysis are presented in Fig. 6 and 7.

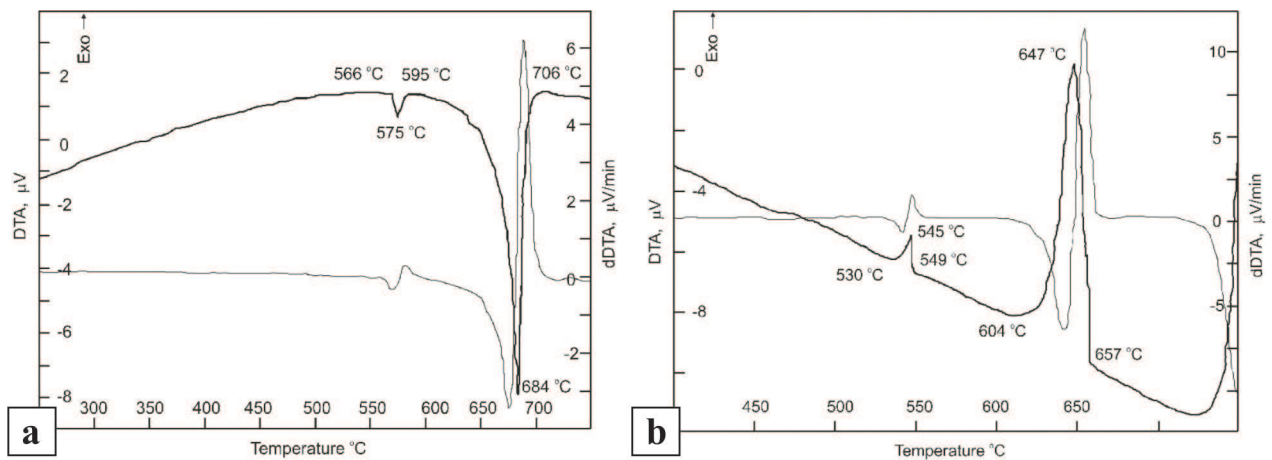


Fig. 5. DTA curves for MSR-B alloy: a) heating b) cooling

### 3. Results and discussion

The analysis of heat flow and DTA curves for the MSR-B alloy during heating (Fig. 5a) and during cooling (Fig. 5b) made it possible for us to determine the liquidus and solidus temperatures. For the MSR-B alloy the liquidus temperature  $T_L$  is 706°C, and the solidus temperature  $T_S$  is 530°C. The range of liquid phase occurrence is thus 176°C.

Ductility tests of the MSR-B alloy conducted on a Gleeble 3800 simulator made it possible to measure the temperatures characteristic for the brittle temperature range. The nil-strength temperature – NST was calculated as an average temperature of five samples in which cracks occurred. Tests were conducted for all conditions of the material (Table 1). For the as-received MSR-B alloy this temperature was 537°C, and after solution heat treatment and precipitation hardening it increased to 545°C (Table 2). The structure and the fracture surface are shown in Fig. 6.

TABLE 2

NST test results for MSRB alloy

Alloy	Material condition	TNST
MSR-B	initial state	537°C
	Treatment alternative I	545°C
	Treatment alternative II	545°C

The value of the NST temperature is a significant feature of the material, because it defines its solidifica-

tion cracking susceptibility, both during casting, as well as during welding [3]. It means, that after exceeding this value the material or welded joint is no longer able to transfer load.

The as-received MSR-B alloy is characterised by the structure of solid solution crystals ( $\alpha$ ) with separated eutectic in the form of a lattice [1]. Based on results of microanalysis of chemical composition (EDS) (Fig. 7) and results of X-ray diffraction (XRD) it was found that the intermetallic phase correspond to  $(Mg, Ag)_{12}Nd$ .

The NST temperature in this state is 537°C. Metallographic analysis shows that the resistance loss of the alloy at high temperatures occurs in the form of disruption of liquid film on crystallite boundaries (Fig. 8a). A liquid film forms as a result of melting of the eutectic  $[Mg(\alpha) + (Mg, Ag)_{12}Nd]$ , which next, during cooling, crystallises on the surface of crystals (fig. 8b). Destruction of the alloy after solution heat treatment also starts at contact places of three solid solution crystals  $Mg(\alpha)$ (Fig. 8c). However, due to the significantly lower amount of eutectic (below 1%), the NST temperature is 545°C (Table 2). In this case the eutectic flash lands between the crystallites were observed, which proves the presence of the healing process (Fig. 8d). Similar mechanism was observed in the alloy after solution heat treatment and ageing. Microstructure analysis shows that alloy cracking occurs as a result of eutectic melting on boundaries of solid solution crystals and its tearing (Fig. 8e,f). The NST temperature for the MSR-B alloy after full heat treatment is also 545°C, which proves similar cracking mechanisms as for alloy after solution heat treatment.

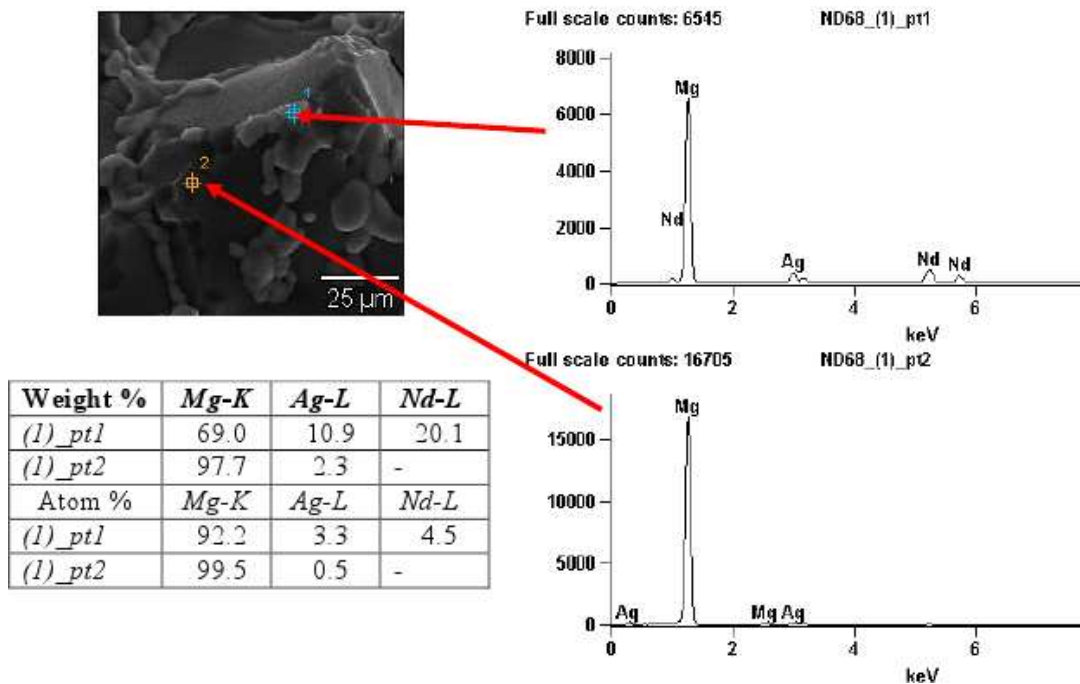


Fig. 6. Results of microanalysis EDS of intermetallic phase in MSR-B weld

The nil-ductility temperature – NDT and the ductility recovery temperature – DRT were designated to determine the brittle temperature range. Results of the NDT test are presented in table 3 and the DRT test results are presented in Table 4. The BTR was designated

as the difference between the DRT and NST according to methodology presented in the paper [4]. The results of structure and fracture examination after the NDT test are shown in Fig. 9 and after the DRT test – in Fig. 10.

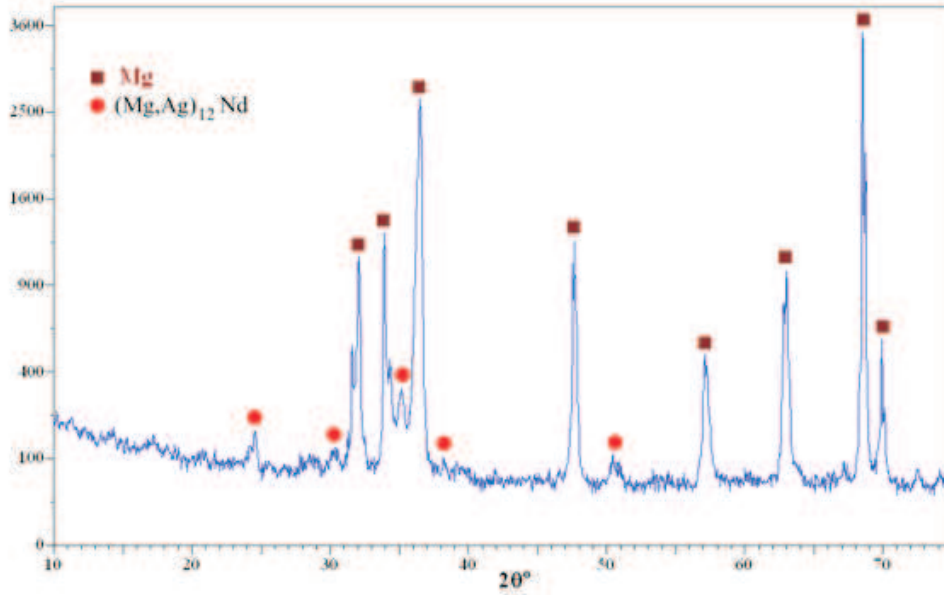


Fig. 7. The result of phase analysis performed by XRD method of MSR-B weld

TABLE 3

Parameters and results of NDT test for the MSR-B alloy

Alloy	HT	$V_o$ , mm/s	$\Delta l$ , mm	Z, %	$R_m$ , MPa	NDT, °C	$R_f$
MSR-B	–	1	0.7	1.6	50	535	0.31
		20	0.4	2.8	55	530	0.32
	I	1	0.4	2.4	47	535	0.31
		20	0.5	1.3	60	525	0.33
	II	1	0.8	2.8	51	535	0.31
		20	0.5	2.9	69	530	0.32

where: HT – heat treatment according to table 1,  $V_o$ – strain speed, NDT- nil-ductility temperature ,  $R_f$ – coefficient of solidification cracking resistance

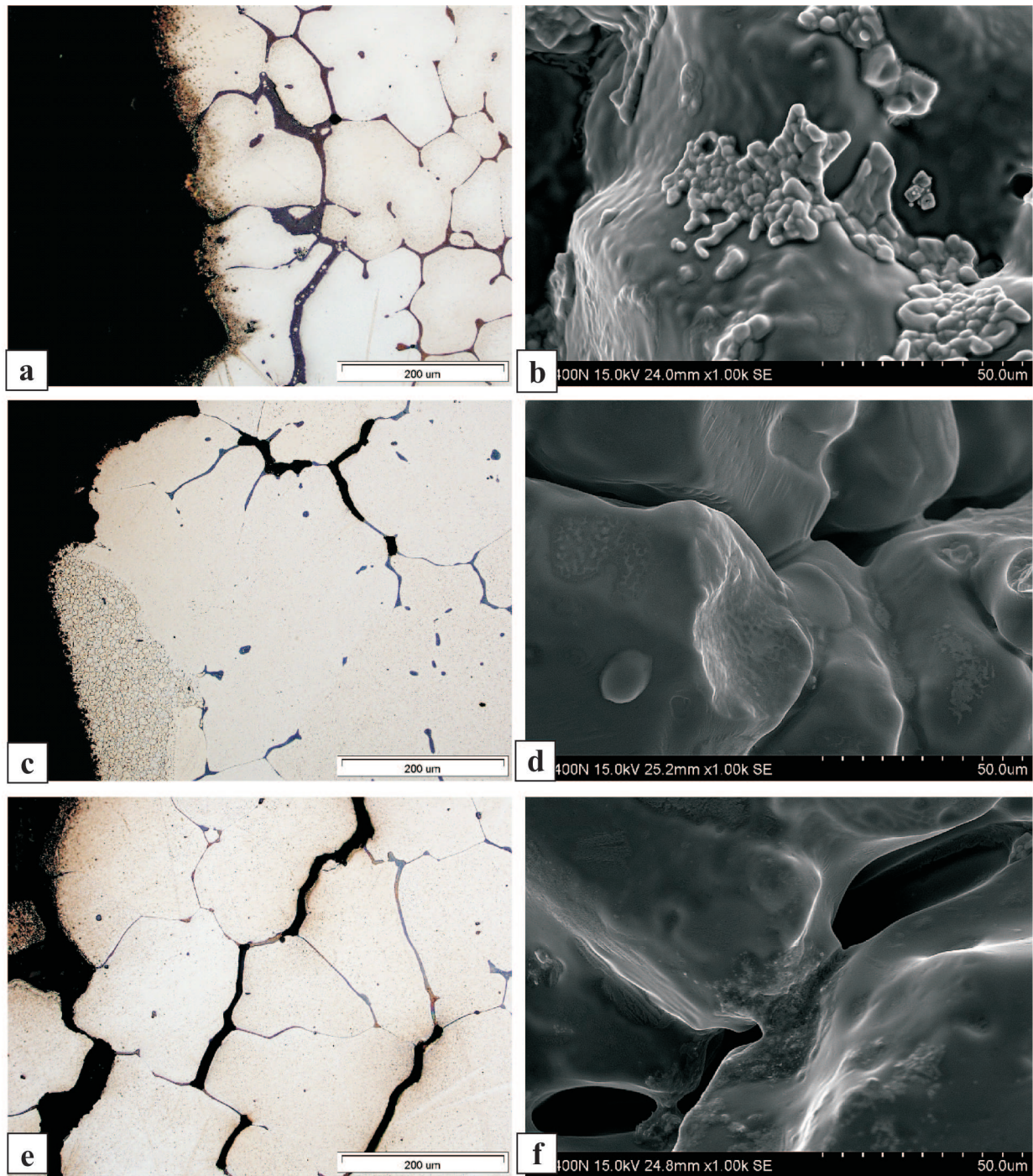


Fig. 8. Microstructure of the crack area of MSR-B alloy after NST test: a) microstructure of the area perpendicular to the alloy fracture surface in initial state with inter-crystalline cracks casted during healing process, LM, b) phase precipitations of  $[\text{Mg}(\alpha) + (\text{Mg}, \text{Ag})_{12}\text{Nd}]$  on the surface of alloy fracture in initial state, SE image, c) inter-crystalline crack in melted phase area  $[\text{Mg}(\alpha) + (\text{Mg}, \text{Ag})_{12}\text{Nd}]$  of alloy after solution heat treatment (OC I), LM, d) bridges between crystals(OC I), SE, e) inter-crystalline cracks with bridges of phase  $[\text{Mg}(\alpha) + (\text{Mg}, \text{Ag})_{12}\text{Nd}]$  (OC II), LM, f) fracture surface of eutectic bridge (OC II), SE

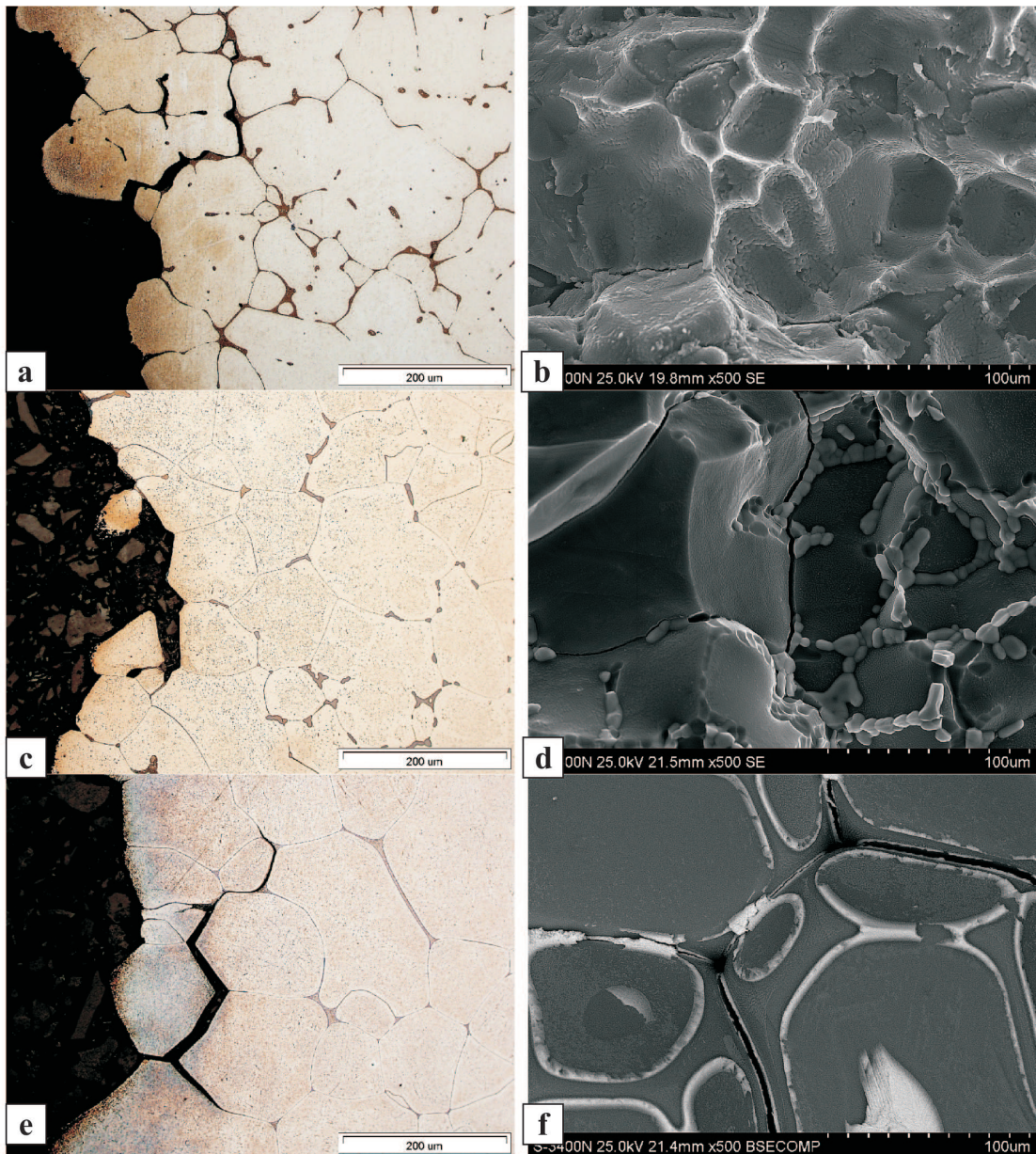


Fig. 9. Microstructure after NDT test for MSR-B: a) lattice of inter-crystalline cracks, alloy in initial state, LM, b) fracture surface covered with  $(\text{Mg, Ag})_{12}\text{Nd}$  solidified phase, as-received material, SE image, c) microstructure of the damage area of alloy after solution heat treatment, crack along crystallite boundaries  $\text{Mg}(\alpha)$  (OC I), LM, d) topography of the alloy fracture after solution heat treatment with visible crack along crystallite boundaries and phase division  $(\text{Mg, Ag})_{12}\text{Nd}$  (OC I), SE, e) after-fracture crack along crystallite boundaries of the solid solution of alloy after solution heat treatment and ageing (OC II), LM, f) fracture surface with visible traces of solidified and cracked phase  $(\text{Mg, Ag})_{12}\text{Nd}$  and cracks along crystallite boundaries, (OC II), SE

The designated NDT temperature for the as-received MSR-B alloy is respectively  $490^{\circ}\text{C}$  for strain rate of 0.008 1/s and  $515^{\circ}\text{C}$  with speed of 0.16 1/s (Table 3). Microstructure analysis on the surface perpendicular to the fracture shows that the crack appears in areas of melted separated eutectic  $[\text{Mg}(\alpha) + (\text{Mg, Ag})_{12}\text{Nd}]$  and develops along the lattice of this eutectic (Fig. 9a). Fractographic testing of the fracture show on the surface of solid solution crystals  $\text{Mg}(\alpha)$  the crystallised inter-metallic

phase  $(\text{Mg, Ag})_{12}\text{Nd}$ . It confirms the fact that a crack develops through division of liquid from the melted separated eutectic (Fig. 9). After solution heat treatment the NDT temperature rises to  $515^{\circ}\text{C}$  with strain rate of 0,008 1/s and  $500^{\circ}\text{C}$  for strain rate of 0.16 1/s (Table 3). It is caused by lower content of the separated eutectic, which in the alloy after solution heat treatment remains only in triple points (Fig. 9c). Solidification crack appears in this area and next develops along boundaries of the

magnesium solid solution  $Mg(\alpha)$  (Fig. 9d). Analysis of solidification cracking of the MSR-B alloy after solution heat treatment and ageing shows, that also in this case the areas of separated eutectic [ $Mg(\alpha) + (Mg, Ag)_{12}Nd$ ] there are areas where cracks appear. Melting of the eutectic occurs and as a result of disruption of the liquid film a separation of crystallised solid solution crystallites  $Mg(\alpha)$  occurs (Fig. 9e), as confirm by observations of the fracture (Fig. 9f). It was found out that on the crystals

surface  $Mg(\alpha)$  the residue of the liquid with chemical composition of the phase  $(Mg, Ag)_{12}Nd$  crystallise.

It was concluded then, that heat treatment results in an extension of the range between NST and NDT temperatures. A slight influence of strain speed on BTR for alloy after heat treatment on solidification cracking was also shown, which is confirmed by the value of coefficient of the resistance to cracking  $R_f$ , which increases from 0.37 to 0.41 (Table 3).

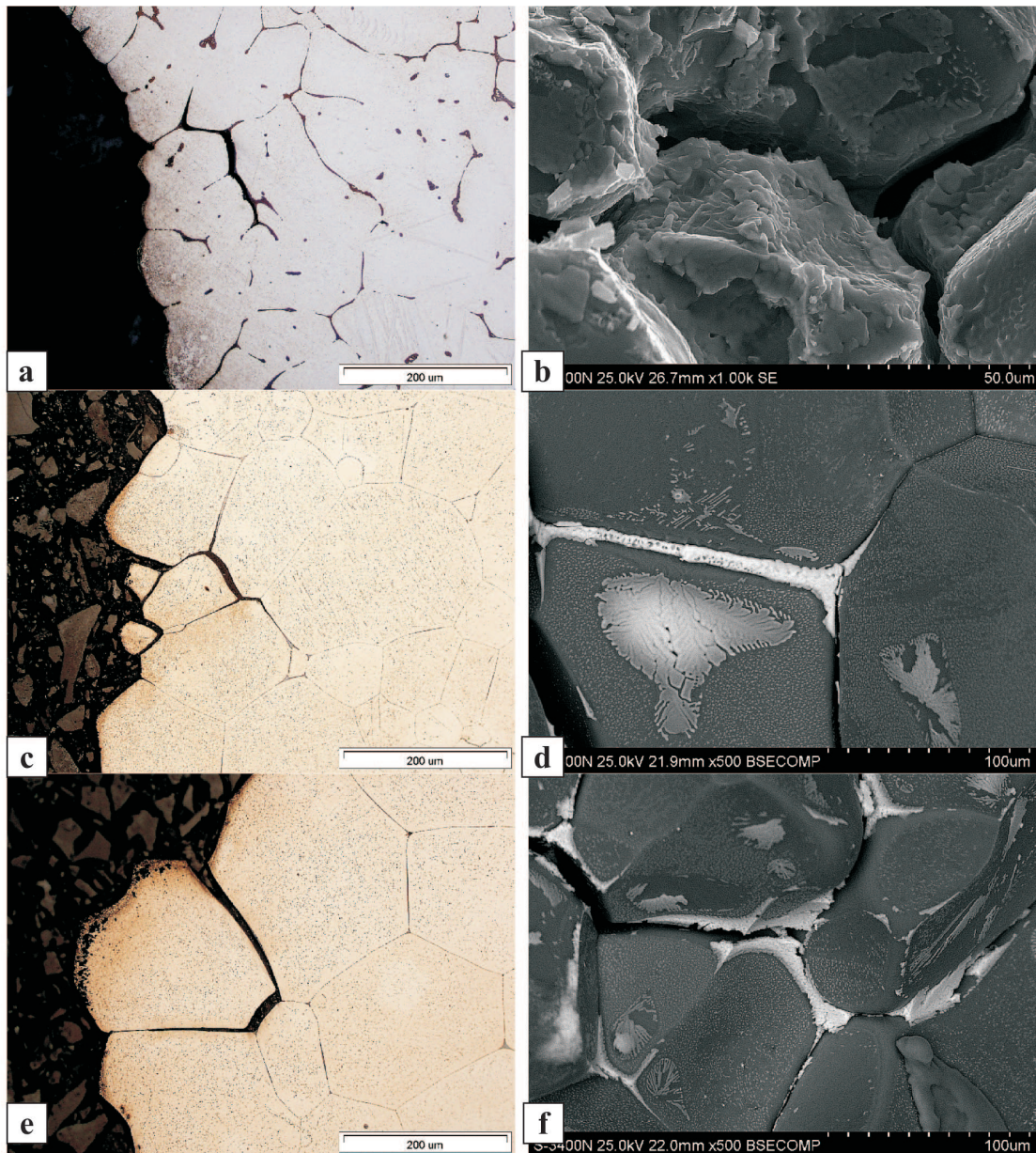


Fig. 10. Microstructure after DRT test for MSR-B: a) microstructure of the area perpendicular to fracture of alloy in initial state, LM, b) surface of alloy fracture in initial condition, SE picture, c) microstructure of crack area after solution heat treatment (OC I), LM, d) topography of the alloy fracture after solution heat treatment (OC I), SE, e) surface perpendicular to alloy fracture after solution heat treatment and ageing (OC II), LM, f) fracture surface (OC II), SE

Parameters and DRT test results for MSR-B alloy

Alloy	HT	$V_o$ , mm/s	$\Delta l$ , mm	Z, %	$R_m$ , MPa	NST, °C	DRT, °C	BTR °C	$\Delta BTR$ , °C
MSR-B	-	1	1,0	2,3	39	568	515	515-568	53
		20	0,3	1,9	54		525	525-568	43
	I	1	0,4	0,8	55	576	520	520-576	56
		20	0,5	2,3	44		505	505-576	71
	II	1	0,8	2,9	49	577	520	520-577	57
		20	1,0	2,1	66		510	510-577	67

where: OC – heat treatment according to table 1,  $V_o$  – strain speed NST – nil-strength temperature, DRT – ductility recovery temperature, BTR – brittle temperature range,  $\Delta BTR$  – brittle temperature range width

Figure 9 presents graphs showing the changes in stress and strain in MSR-B alloy during cooling and heating in temperature function with strain rate of 0.16 1/s.

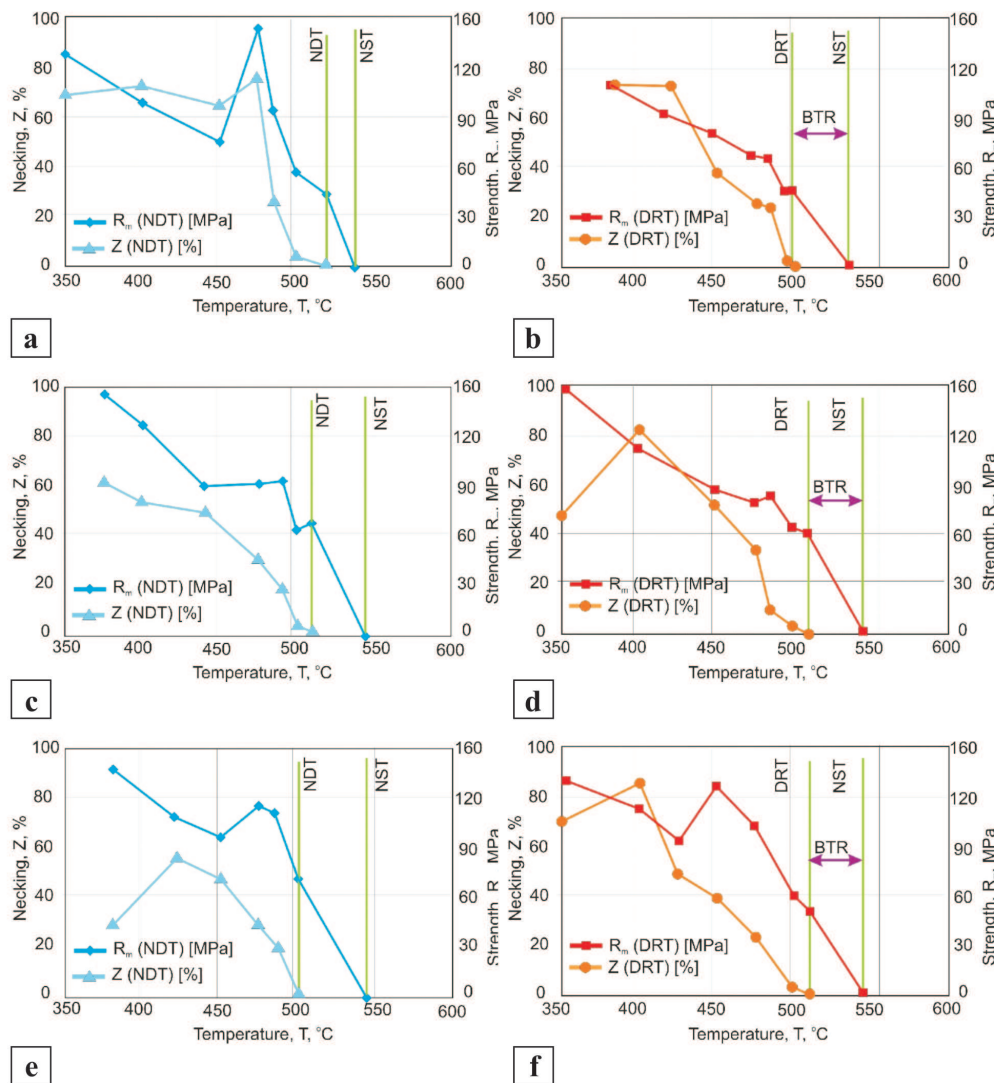


Fig. 11. Contraction and resistance of MSR-B alloy in temperature function: a) material in initial condition, heating, NDT test, b) material in initial condition, cooling, DRT test, c) material after solution heat treatment (OC I), heating, NDT test, d) material after solution heat treatment (OC I), cooling, DRT test, e) material after solution heat treatment and ageing (OC II), heating, NDT test, f) material after solution heat treatment and ageing (OC II), cooling, DRT test

The ductility recovery temperature DRT for the as-received MSR-B alloy is 500°C with strain speed of 1 mm/s and 495°C for strain rate of 0.16 1/s. Solidification cracks in this case appear in melted eutectic [Mg( $\alpha$ ) + (Mg, Ag)<sub>12</sub>Nd)] and form on wet crystallite boundaries Mg( $\alpha$ ) (Fig. 10a). Melted phase (Mg, Ag)<sub>12</sub>Nd) crystallises on the crystal surface and cracks as a result of shrinkage (Fig. 10b). Brittleness range for the MSR-B alloy without heat treatment is 37°C, that is from 500°C to 537°C (Table 4, Fig 11b).

The alloy, after solution heat treatment in temperature of 525°C for 8 hours, cracks in DRT test by separation of crystal crystallites Mg( $\alpha$ ) on the film of liquid inter-metallic phase. The crack has the character of an inter-crystalline lattice (Fig. 10c). On the surface of fracture the phase (Mg, Ag)<sub>12</sub>Nd) was found, precipitating in inter-crystalline spaces and on the crystallite surfaces (Fig. 10b). Similar phenomenon was observed in the alloy after complete heat treatment (Fig. 10e,f). It appears that during cooling cracks appear as a result of disruption of the liquid film between the crystallised solid solution crystallites ( $\alpha$ ) (Fig. 10f). It was observed, that during lowering of the temperature below the solidus temperature the disruption occurs of the crystallised phase bridges (Mg, Ag)<sub>12</sub>Nd) (Fig. 10f).

Achieved results explicitly show the dependence between the BTR range and the strain speed. Brittle temperature range for MSR-B alloy with strain rate of 0.008 1/s is 40°C, whereas with strain of 0.16 1/s is 47°C. The BTR for the MSR-B alloy after heat treatment, both after solution heat treatment and after solution heat treatment and ageing is on similar level. It is respectively 35-45°C for strain speed of 1 mm/s and 40°C for strain rate of 0.16 1/s (Table 4). It can be concluded then, that the strain speed increase results in widening the brittle temperature range. Moreover, it was found out, that heat treatment does not influence the brittle temperature range (Fig. 11b,d,f).

#### 4. Conclusions

On the basis of the conducted tests and results analysis the following conclusions were derived:

- The developed methodology of the resistance to solidification cracking of the MSR-B alloy makes it

possible for us to describe the brittle temperature range (BTR) and at the same time allows us the right choice of technological and construction parameters providing the productions of alloys without defects.

- Brittle temperature range is considered as a difference between the nil-ductility temperature and ductility recovery temperature for the as-received MSR-B alloy with strain rate of 0,008 1/s is 40°C and for strain rate of 0,16 1/s is 47°C. Similar values of BTR were found after heat treatment of the alloy (from 35°C to 45°C). Moreover, it was found out that the increase of strain speed causes a slight increase in BTR width of about 5°C.
- Solidification cracks in MSR-B alloy are initiated in the areas of melted separated eutectic [Mg( $\alpha$ ) + (Mg, Ag)<sub>12</sub>Nd)] and develop on boundaries of solid solution crystallites Mg( $\alpha$ ) as a result of disruption of liquid film. A healing mechanism, consisting in pouring liquid to appearing cracks, was disclosed, however, as a result of strains and crystalline stresses of the inter-metallic phase (Mg, Ag)<sub>12</sub>Nd) they crack.
- Marked temperatures from brittle temperature range: nil-strength temperature NST (537°C), nil-ductility temperature NDT during heating (515°C), ductility recovery temperature DRT during cooling (495°C) and resistance to cracking coefficient  $R_f$  on a level of 0.4 are directions for engineers when designing technologies of casting and repairing MSR-B alloys.

#### REFERENCES

- [1] D.G. Eskin in. Mechanical properties in the semi-solid state and hot tearing of aluminium alloys, *Progress in Materials Science* **49**, 5, 629-711 (2004).
- [2] T.W. Clyne, G.J. Davies, In: *Solidification and casting of metals* London: Metals Society; 275 (1979).
- [3] T. Bollinghaus, H. Herold, *Hot cracking phenomena in welds*, Springer (2005).
- [4] *Gleeble 3800 Applications, Welding Process Simulation*, (2000).
- [5] A. Kiełbas, Structure and mechanical properties of casting MSR-B magnesium alloy; *Journal of achievements in materials and manufacturing engineering* **18**, 1-2, 131-134 (2006).